Analysis of Titanium Doping Effects on Structural, Optical and Gas-Sensing Properties of Cobalt Oxide Nanostructured Thin Films

Maab Falah Hasan[1], Muthanna Fakhri Allawaia[1], Abdul-Lateef Abdul-Jabar[2], Muhaned Zaidi[3], Dalia Akram Mahmood[4] and Muhannad Jadan[5]
[1]Department of Medical Physics, College of Applied Science, University of Fallujah, 31002 Fallujah, Iraq
[2]Department of Physics, College of Education, Mustansiriyah University, 10052 Baghdad, Iraq
[3]Department of Medical Physics, College of Science, Al-Manara University, 62001 Amarah, Iraq
[4]Department of Physics, College of Science, Mustansiriyah University, 10052 Baghdad, Iraq
[5]Department of Applied Physics, Faculty of Science, Tafila Technical University, PO Box 179, 66110 Tafila, Jordan
lateefl991@uomustansiriyah.edu.iq

Keywords: Co_3O_4, Chemical Spray Pyrolysis, Titanium Doping, Thin Films, Structural Properties, Optical Band Gap, NO_2 Gas Sensing.

Abstract: This study investigates the role of Ti doping on the properties of Co_3O_4 nanostructured thin films deposited via chemical spray pyrolysis on glass substrates at 400 °C. X-ray diffraction analysis confirmed a polycrystalline spinel cubic structure with a predominant (220) orientation. Crystallite size increased from 12.91 nm for undoped films to 24.13 nm for 4% Ti-doped samples, indicating enhanced grain growth. Atomic force microscopy revealed reduced surface roughness and particle size with Ti incorporation, suggesting improved film uniformity. Optical measurements demonstrated high visible transmittance (85.5–80.6%) and a bandgap narrowing from 2.68 to 2.58 eV, attributed to defect-state formation within the band structure. Additionally, absorption and extinction coefficients varied with doping concentration, while the refractive index exhibited a decreasing trend. Gas sensing tests toward NO_2 at 100 °C showed a progressive sensitivity decline with increasing Ti content, implying that doping adversely affects the sensing response. Overall, these findings indicate that Ti incorporation systematically tailors the structural, morphological, optical, and gas-sensing characteristics of Co_3O_4 thin films.

1 INTRODUCTION

In public safety, human health, emissions management, and environmental protection, sensors are crucial [1]-[3]. For almost 50 years, research on metal oxide semiconductor (MOS) gas sensors has been conducted [4]-[8]. MOS sensors can detect flammable or poisonous gases, such as CO, NO_2, CH_4, and VOCs [9]-[11]. Their process is based on the adsorption of reducing or oxidizing gases on MOS films, which alters electrical conductivity [12], [13]. Due to its unique electrical and visual electrocatalytic capabilities, cobalt oxide (Co_3O_4), a significant transition-metal oxide, has played a key role in research efforts [14]-[16]. Because of its straight optical band gaps of roughly 1.48 and 2.19 eV, it has significant potential for use in gas sensors, catalysts, and optoelectronic devices [17]-[20]. Adapting Co_3O_4 with appropriate dopants has been considered a viable way to improve both structural and functional qualities in recent years [21], [22]. Doping titanium in this way has been proposed as a potential means to alter the physical and sensing properties of metal oxides [23]. In addition to increasing the number of active surface sites and the sensing material's contact with target gases, these modulations can facilitate charge transport [24]. Adsorbed oxygen species from the atmosphere usually line the surface of metal oxide semiconductors. These oxygen molecules cause p-type semiconductors to form a hole-accumulation layer and n-type semiconductors to form an electron-depletion layer, as they trap electrons in the material [25], [26]. This research aimed to investigate how Ti doping alters the physical properties of CoO_4 and enhances the material's sensing capabilities across a range of applications.

2 EXPERIMENTAL

CSP was used to deposit undoped cobalt oxide and Co3O4:Ti thin films on glass substrates. Cobalt chloride (0.1 M) is present in the solution. 2% and 4% of (Co (CH3COO)2·2H2O) was used as a dopant agent. To obtain Ng of 1% and 3%, 0.1 M of titanium chloride (TiCl2.6H2O) was used as the doping material. Following numerous experiments, the ideal conditions were determined to be 400°C for the substrate and 30 cm between the spout and the substrate. To avert cooling, the spray rate was 8 seconds, followed by 1.30 minutes, with an average flux of 6 mm³/min. Nitrogen was the carrier gas. Cu Kα radiation (λ = 0.15406 nm) was applied in XRD (Shimadzu, model: XRD-6000, Japan) to determine structural data. The surface morphology of the deposited thin films was characterized by atomic force microscopy (AA 3000 Scanning Probe Microscope). The UV-Vis spectrometer instrument analyses transmittance and absorbance spectra over the 300-900 nm wavelength range. A cylindrical cylinder, 17 cm high and 8.5 cm in radius, is commonly used to measure gas sensitivity.

3 RESULTS AND DISCUSSION

Figure 1 presents the X-ray diffraction (XRD) patterns of pure and Ti-doped Co3O4 thin films deposited by chemical spray pyrolysis (CSP) at 400 °C. Four dominant diffraction peaks are observed at 20.27°, 31.76°, 38.97°, and 68.87°, corresponding to the (111), (220), (222), and (351) crystallographic planes, respectively. These reflections are consistent with the standard JCPDS card No. 42-164, confirming the successful formation of polycrystalline Co3O4 with a cubic spinel crystal structure. Among the observed reflections, the (220) plane exhibits the highest intensity, indicating a preferred growth orientation.

The structural parameters obtained from the XRD analysis are summarized in Table 1. The crystallite size increases from 12.91 nm for the undoped Co3O4 film to 17.05 nm and 24.13 nm for the films containing 2% and 4% Ti, respectively. This increase indicates that titanium incorporation promotes crystal growth and enhances the crystallinity of the deposited films [28].

The dislocation density decreases from 67.41 × 10^{14} to 40.95 × 10^{14} lines/m² as the Ti concentration increases, indicating a reduction in crystal defects and an improvement in the crystalline quality of the films [29], [30]. Similarly, the lattice strain decreases from 31.72 × 10^{-4} for the undoped Co3O4 film to 24.32 × 10^{-4} for the film containing 4% Ti. The reduction in lattice strain suggests improved structural ordering resulting from the incorporation of Ti ions into the Co3O4 lattice [31], [32]. The corresponding structural parameters are listed in Table 1, while Figure 2 illustrates the variation of FWHM, crystallite size, lattice strain, and dislocation density with Ti concentration.

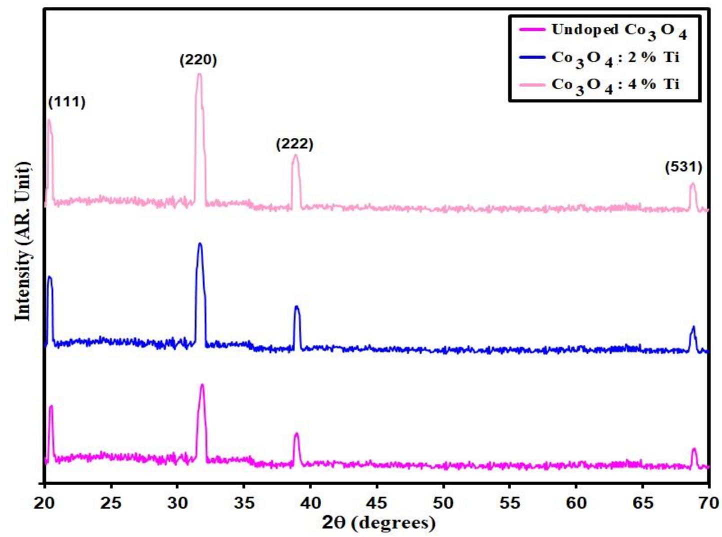

Figure 1: X-ray diffraction (XRD) patterns of pure and Ti-doped Co_3O_4 thin films.

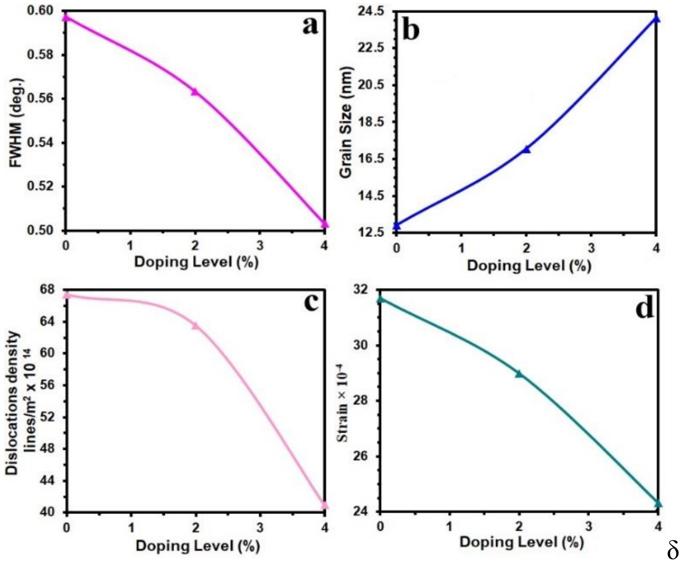

Figure 2: Structural parameters of pure and Ti-doped Co_3O_4 thin films: a) FWHM, b) crystallite size (D), c) lattice strain (ε), and d) dislocation density (δ).

Table 1: Structural parameters of pure and Ti-doped Co_3O_4 thin films..

Specimen	2 θ (°)	(hkl) Plane	FWHM (°)	E_g (eV)	*D* (nm)	$\delta \times 10^{14}$ (lines/m²)	ε ×10⁻⁴
Co_3O_4	31.76	220	0.59	2.68	12.91	67.41	31.72
Co_3O_4: 2% Ti	31.74	220	0.56	2.63	17.05	63.52	28.98
Co_3O_4: 4% Ti	31.70	220	0.50	2.58	24.13	40.95	24.32

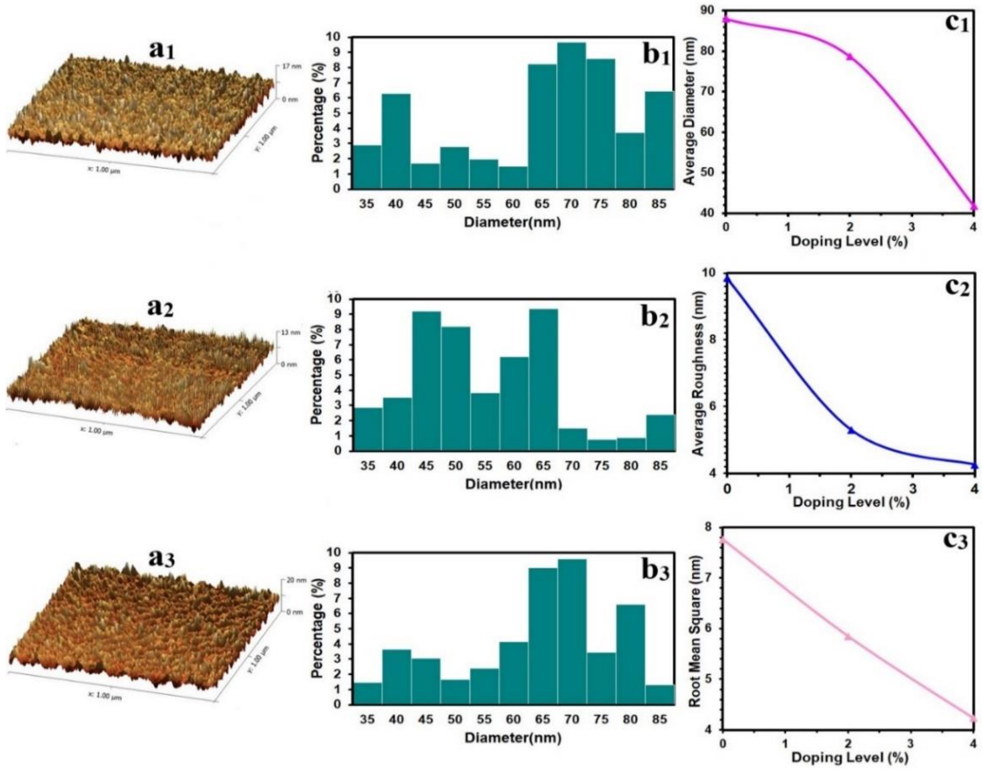

Figure 3: AFM surface morphology of pure and Ti-doped Co_3O_4 thin films.

The surface morphology of the pure and Ti-doped Co3O4 thin films was examined using atomic force microscopy (AFM), and the corresponding images are presented in Figure 3. All films exhibit a homogeneous nanostructured granular morphology with uniformly distributed grains across the surface. The average particle size decreases from 88.0 nm for the undoped film to 41.8 nm for the film containing 4% Ti, indicating that Ti incorporation suppresses particle growth. The extracted AFM parameters are summarized in Table 2. The average surface roughness (Ra) decreases from 9.85 nm for the undoped film to 5.30 nm and 4.25 nm for the films containing 2% and 4% Ti, respectively. Likewise, the root-mean-square (RMS) roughness decreases from 7.76 nm to 5.85 nm and 4.23 nm with increasing Ti concentration. The reduction in particle size and surface roughness indicates that Ti incorporation modifies the nucleation and growth mechanisms during film deposition, resulting in denser and more uniform Co3O4 thin films [33].

Table 2: AFM parameters of pure and Ti-doped Co_3O_4 thin films.

Samples	P_{av} nm	R_a nm	RMS nm
Co_3O_4	88.0	9.85	7.76
Co_3O_4: 2% Ti	78.7	5.30	5.85
Co_3O_4: 4% Ti	41.8	4.25	4.23

The optical transmittance spectra of the pure and Ti-doped Co3O4 thin films are presented in Figure 4. All films exhibit high optical transparency in the visible region, with transmittance values ranging from 82.5% to 85.6%, indicating good optical quality and uniform film deposition. Furthermore, the transmittance increases toward longer wavelengths in the near-infrared region, suggesting reduced photon absorption at lower photon energies [34].

Figure 5 shows the optical absorbance spectra of the pure and Ti-doped Co3O4 thin films. The undoped Co3O4 film exhibits the lowest absorbance, whereas the absorbance gradually increases with increasing Ti concentration. This enhancement is attributed to Ti-induced modifications of the electronic structure and the formation of localized energy states that promote photon absorption within the films [35]–[38].

The absorption coefficient spectra are presented in Figure 6. The absorption coefficient increases with increasing Ti concentration, reaching values on the order of 10^4 cm^{-1}, indicating strong optical absorption by the deposited films [39]. A pronounced increase is observed near the absorption edge, followed by a gradual decrease at higher photon energies. This behavior is characteristic of direct interband electronic transitions and confirms the excellent optical absorption capability of the Ti-doped Co3O4 thin films [40], [41].

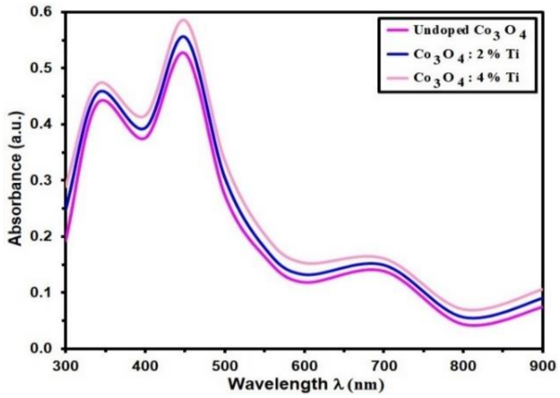

Figure 4: Optical absorbance spectra of pure and Ti-doped Co_3O_4 thin films.

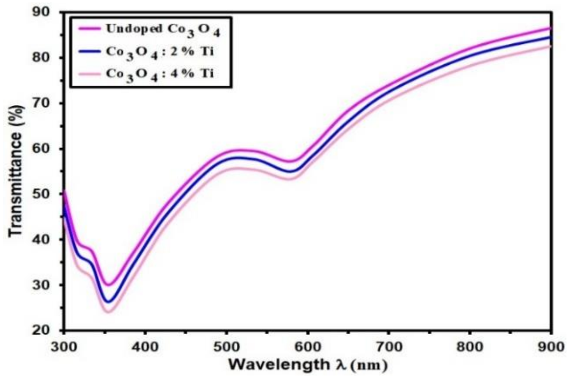

Figure 5: Optical transmittance spectra of pure and Ti-doped Co_3O_4 thin films.

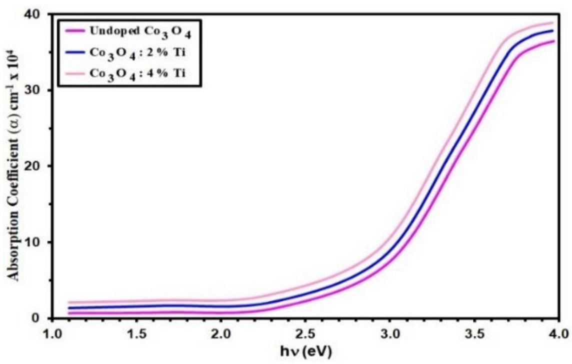

Figure 6: Absorption coefficient spectra of pure and Ti-doped Co_3O_4 thin films.

The optical band-gap values derived from the absorption spectra are presented in Figure 7. The band gap decreases gradually from 2.68 eV for the undoped

Co3O4 film to 2.58 eV for the film containing the highest Ti concentration. This reduction is attributed to the formation of Ti-induced impurity and defect states within the forbidden band gap, which facilitate electronic transitions at lower photon energies [42]–[44]. The observed changes in both the absorption coefficient and the optical band gap demonstrate that Ti incorporation effectively modifies the electronic band structure of Co3O4 thin films.

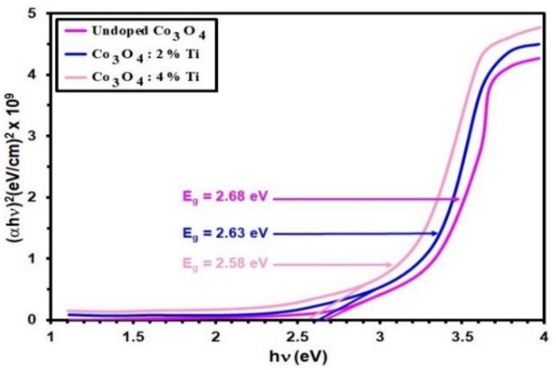

Figure 7: Optical band-gap (Tauc) plots of pure and Ti-doped Co_3O_4 thin films.

Figure 8 presents the extinction coefficient spectra of the pure and Ti-doped Co3O4 thin films. The extinction coefficient increases rapidly in the ultraviolet region and then gradually decreases with increasing wavelength. The non-zero extinction coefficient below the fundamental absorption edge indicates the presence of localized defect states and impurity levels that contribute to sub-band-gap optical absorption [45], [46].

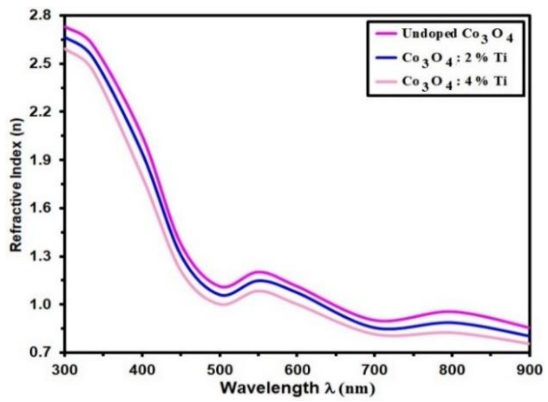

Figure 8: Refractive index spectra of pure and Ti-doped Co_3O_4 thin films.

The variation of the refractive index with wavelength is shown in Figure 9. The refractive index decreases systematically with increasing Ti concentration throughout the investigated spectral range. This behavior is attributed to changes in the electronic polarizability and structural modifications induced by Ti incorporation into the Co3O4 lattice [47]–[49].

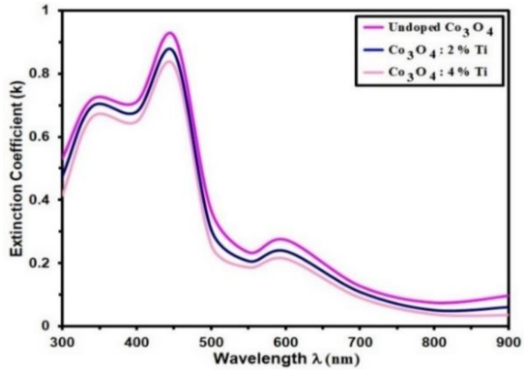

Figure 9: Extinction coefficient spectra of pure and Ti-doped Co_3O_4 thin films.

The gas-sensing performance of the fabricated films was evaluated at an operating temperature of 100 °C, which was selected based on preliminary measurements showing the highest sensor response. Figure 10 presents the dynamic resistance response of the pure and Ti-doped Co3O4 thin films upon exposure to 240 ppm NO_2 gas. The undoped Co3O4 film exhibits the lowest electrical resistance, indicating more effective adsorption of NO_2 molecules on its surface. In contrast, the electrical resistance increases with increasing Ti concentration, reaching its highest value for the film containing 4% Ti. This behavior is attributed to Ti-induced modifications of the electronic structure and the interaction between the sensing surface and NO_2 molecules, which reduce charge-carrier mobility and consequently increase the electrical resistance [50]–[54].

Figure 11 illustrates the NO_2 gas-sensing sensitivity of the pure and Ti-doped Co3O4 thin films. The sensitivity decreases systematically with increasing Ti concentration [55], [56]. Specifically, the sensitivity decreases from 45.97% to 21.57% at 140 ppm, from 47.80% to 22.89% at 190 ppm, and from 49.31% to 24.65% at 240 ppm as the Ti concentration increases from 0% to 4%. This reduction is attributed to changes in the electronic structure, reduced charge transfer efficiency, and enhanced charge-carrier recombination, which decrease the number of free carriers available for gas detection and consequently weaken the sensing performance of the Ti-doped Co3O4 thin films [57].

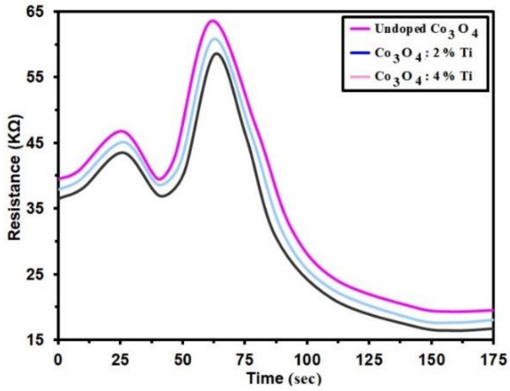

Figure 10: Dynamic resistance response of pure and Ti-doped Co_3O_4 thin films toward NO_2 gas.

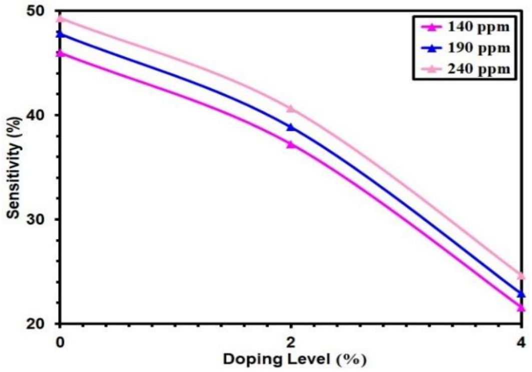

Figure 11: NO_2 gas-sensing sensitivity of pure and Ti-doped Co_3O_4 thin films.

4 CONCLUSIONS

Crystallite size in our study went from 12.91 nm (undoped) to 24.13 nm (4% Ti) which also saw dislocation density and microstrain go down which in turn improved crystalline quality. Also we saw via atomic force microscopy that surface roughness went down and average particle size decreased with increase in Ti content which in turn improved film uniformity. Also we found via optical characterization that we have high transmittance in the visible region (85.5–80.6%) and a direct band gap which reduced from 2.68 to 2.58 eV which we attribute to Ti induced defect states. Also we noted that the absorption coefficient went up with doping but the refractive index went down. At gas sensing we looked at NO_2 at 100 °C and saw that sensitivity went down as we increased Ti doping which we think is due to titanium's effect on the electronic structure.

ACKNOWLEDGMENTS

Mustansiriyah University supports this effort (www.uomustansiriyah.edu.iq).

REFERENCES

[1] S. A. Alavi-Borazjani and M. N. Shafique, "Chemical sensors for hazardous substances: advances in design, materials, and applications in environmental monitoring," Environmental Monitoring and Assessment, vol. 198, no. 1, p. 33, 2026.

[2] S. Ahmed, A. Pasha, T. Kumer, M. Akhtaruzzaman, and M. Hossain, "Advancements in Air Quality Monitoring Systems: A Comprehensive Review of Emerging Technologies for Enhancing Environmental Health," Indoor Air, vol. 2026, no. 1, Art. no. 3080684, 2026.

[3] B. Shingan, M. Pujari, and A. K. Aarya, "Advancing environmental safety in city gas distribution: sustainable solutions and infrastructure resilience," Sustainable and Resilient Infrastructure, vol. 11, no. 1, pp. 55-78, 2026.

[4] N. Goel, K. Kunal, A. Kushwaha, and M. Kumar, "Metal oxide semiconductors for gas sensing," Engineering Reports, vol. 5, no. 6, Art. no. e12604, 2023.

[5] L. X. Ou, M. Y. Liu, L. Y. Zhu, D. W. Zhang, and H. L. Lu, "Recent progress on flexible room-temperature gas sensors based on metal oxide semiconductor," Nano-Micro Letters, vol. 14, no. 1, p. 206, 2022.

[6] A. G. Patil, B. Pramanick, and A. Madhukar, "MOS-based gas sensors for monitoring of air pollution: A review," IEEE Sensors Journal, vol. 25, no. 6, pp. 9250-9262, 2025.

[7] P. M. Bulemo, D. H. Kim, H. Shin, H. J. Cho, W. T. Koo, S. J. Choi, et al., "Selectivity in chemiresistive gas sensors: strategies and challenges," Chemical Reviews, vol. 125, no. 8, pp. 4111-4183, 2025.

[8] S. Deepak, P. Anilkumar, J. Jasmin, and S. Preetha, "Room-temperature detection of harmful gases: a comprehensive review of metal oxide nanostructured chemiresistive sensors," Journal of Nanoparticle Research, vol. 27, no. 9, 2025.

[9] J. Wang, H. Gong, F. Tian, Z. Li, J. Li, J. Jiang, et al., "Chemiresistive Gas Sensors: Materials, Mechanisms, and Applications on the Road to Intelligence and Multifunctionality," Small, Art. no. e12547.

[10] R. Kumar, P. Ghosh, A. Gupta, and C. S. Prajapati, "Highly sensitive and selective ethanol detection at low temperature via Pulse Laser Deposited V_2O_5 thin film," Sensors and Actuators A: Physical, Art. no. 117513, 2026.

[11] L. Chen, Y. J. Wang, X. Q. Kuang, Y. Q. Zhang, T. Y. Yang, M. Li, and Z. Guo, "Hollow Co_3O_4 nanocubes incorporated into porous ZnO nanotubes for selectively enhanced gas sensing toward BTEX," Sensors and Actuators B: Chemical, Art. no. 139488, 2026.

[12] D. Y. Nadargi, A. Umar, J. D. Nadargi, S. A. Lokare, S. Akbar, I. S. Mulla, et al., "Gas sensors and factors influencing sensing mechanism with a special focus on MOS sensors," Journal of Materials Science, vol. 58, no. 2, pp. 559-582, 2023.

[13] J. Wawrzyniak, "Advancements in improving selectivity of metal oxide semiconductor gas sensors opening new perspectives for their application in food industry," Sensors, vol. 23, no. 23, p. 9548, 2023.

[14] D. Majumdar, M. Dutta, and R. Mondal, "Spinels-structured cobalt-based transition metal mixed oxides (MCo_2O_4): evolutionary materials for advanced supercapatteries," Journal of Solid State Electrochemistry, vol. 30, no. 1, pp. 189-232, 2026.

[15] Nasrullah, W. Wisal, F. Bibi, S. K. Shah, J. Ullah, M. Rauf, et al., "Electrospun SnO_2/Co_3O_4 Core-Shell Nanofibers Decorated with ZnO for High Performance Asymmetric Supercapacitors," Journal of Inorganic and Organometallic Polymers and Materials, pp. 1-17, 2026.

[16] V. T. Hoang, D. H. Thuc, N. T. Dao, P. T. Hien, X. D. Ngo, N. Van Tuyen, et al., "Boosting the oxidase-mimicking activity of MnO_2-GO nanohybrids: Elucidating the critical role of graphene oxide on nanozyme catalytic performance," Inorganic Chemistry Communications, Art. no. 116351, 2026.

[17] R. Balaji, P. Mohan, S. Vinoth, M. Hadi, I. M. Ashraf, K. B. Ansari, et al., "Fascinating opto-gas sensors development based on thin films for environmental and optoelectronic devices," Journal of Science: Advanced Materials and Devices, Art. no. 101096, 2026.

[18] A. Hammod, N. J. Ridha, K. J. Tahir, F. K. M. Alosfur, A. S. Yasir, and L. A. Majeed, "Semiconductor Gas Sensors: Metal Oxides, Synthesis Methods, Applications as Gas Sensors, and Oxidation and Reduction Mechanisms," Indonesian Journal of Chemistry, vol. 25, no. 1, pp. 306-332, 2025.

[19] Z. Zhang, P. Qiu, Y. Deng, and W. Luo, "Recent advances in functionalizing metal oxide semiconductors for highly sensitive gas sensors," Small Methods, vol. 9, no. 10, Art. no. 2500228, 2025.

[20] D. K. Chaudhary, Study on Electrical and Optical Properties of Zinc Oxide Semiconductor for Gas Sensor Application, Doctoral dissertation, Amrit Campus, 2023.

[21] A. M. Albarkani, I. H. Alsohaimi, M. S. Alhumaimess, M. Alzaid, Q. Chen, M. A. El-Hashemy, and H. M. Hassan, "Mitigating Electronic Limitations in Co_3O_4 via Rational Dopant Integration for Multifunctional Sustainable Energy Applications: Oxygen Evolution and Photoelectrochemical Water Reduction," Electrochimica Acta, Art. no. 148085, 2025.

[22] P. Akbarian, A. Eshghi, A. Asadi, and M. Kheirmand, "Pd-Co_3O_4/acetylene black nanocomposite as an efficient and robust bifunctional ORR/OER electrocatalyst for rechargeable zinc-air batteries," International Journal of Hydrogen Energy, vol. 91, pp. 1103-1112, 2024.

[23] S. Ramanavicius, A. Jagminas, and A. Ramanavicius, "Gas sensors based on titanium oxides," Coatings, vol. 12, no. 5, p. 699, 2022.

[24] Lee, M. Kim, S. Park, J. Ahn, and I. D. Kim, "Materials Engineering for Light-Activated Gas Sensors: Insights, Advances, and Future Perspectives," Advanced Materials, vol. 37, no. 40, Art. no. e08204, 2025.

[25] A. J. Albarakati and I. A. Matter, "N-type metal oxide semiconductor: materials and their environmental applications," Biointerface Research in Applied Chemistry, vol. 13, Art. no. 519, 2023.

[26] S. Ahmed and S. K. Sinha, "Studies on nanomaterial-based p-type semiconductor gas sensors," Environmental Science and Pollution Research, vol. 30, no. 10, pp. 24975-24986, 2023.

[27] A. A. Khadayeir, R. I. Jasim, S. H. Jumaah, N. F. Habubi, and S. S. Chiad, "Influence of substrate temperature on physical properties of nanostructured ZnS thin films," Journal of Physics: Conference Series, vol. 1664, no. 1, Art. no. 012009, 2020.

[28] B. Karthikeyan and R. Vettumperumal, "Optical and electrochemical properties of pure and Ti-doped CdO nanoparticles for device applications," Materials Science and Engineering: B, vol. 281, Art. no. 115754, 2022.

[29] S. S. Chiad, A. S. Alkelaby, and K. S. Sharba, "Optical conduct of nanostructure Co_3O_4 rich highly doping Co_3O_4:Zn alloys," Journal of Global Pharma Technology, vol. 11, no. 7, pp. 662-665, 2020.

[30] M. B. Jumaa, T. H. Mubarak, and A. M. Mohammad, "Synthesis and characterization of spinel ferrite $Co_{0.8}Fe_{2.2}O_4$ nanoparticle," Journal of University of Anbar for Pure Science, vol. 15, no. 2, pp. 74-82, 2021.

[31] D. M. Mamand, D. S. Muhammad, S. B. Aziz, P. O. Hama, B. A. Al-Asbahi, A. A. Ahmed, and J. Hassan, "Enhanced optical properties of chitosan polymer doped with orange peel dye investigated via UV-Vis and FTIR analysis," Scientific Reports, vol. 15, no. 1, p. 3232, 2025.

[32] Q. M. Al-Bataineh, A. M. Alsaad, A. A. Ahmad, and A. Telfah, "A novel optical model of the experimental transmission spectra of nanocomposite PVC-PS hybrid thin films doped with silica nanoparticles," Heliyon, vol. 6, no. 6, 2020.

[33] N. A. Alghurabi, T. H. Mubarak, A. K. Judran, and B. A. Hasoon, "Two-stage pulsed laser ablation for the production of Ag@TiO2 core-shell nanoparticles with enhanced antimicrobial properties: An in silico study," Plasmonics, vol. 20, pp. 10863-10888, 2025.

[34] N. N. Jandow, N. F. Habubi, S. S. Chiad, I. A. Al-Baidhany, and M. A. Qaeed, "Annealing effects on band tail width, Urbach energy and optical parameters of Fe2O3:Ni thin films prepared by chemical spray pyrolysis technique," International Journal of Nanoelectronics and Materials, vol. 12, no. 1, pp. 1-10, 2019.

[35] W. Li, X. Fang, J. Lyu, G. Wang, C. Ma, and H. Ma, "Co3O4 decorated Ti/TiO2 nanotubes for photogenerated cathodic protection of 304 stainless steel," Chemical Research in Chinese Universities, vol. 37, no. 3, pp. 704-710, 2021.

[36] M. R. N. S. Hamdani, R. N. Singh, and P. J. Chartier, "Co3O4 and Co-based spinel oxides bifunctional oxygen electrodes," International Journal of Electrochemical Science, vol. 5, no. 4, pp. 556-577, 2010.

[37] M. A. Issa and K. A. Aadim, “Optical Emission Spectroscopy of Zinc Oxide Doped Nickel Oxide to Calculate Plasma Parameters Using the Boltzmann Plot Method,” Iraqi Journal of Physics, vol. 23, no. 2, pp. 118-127, 2025.

[38] Y. Taneja, D. Dube, and R. Singh, “Recent advances in elemental doping and simulation techniques: improving structural, photophysical and electronic properties of titanium dioxide,” Journal of Materials Chemistry C, vol. 12, no. 37, pp. 14774-14808, 2024.

[39] A. Ahad, J. Podder, T. Saha, and H. N. Das, “Effect of chromium doping on the band gap tuning of titanium dioxide thin films for solar cell applications,” Heliyon, vol. 10, no. 1, 2024.

[40] M. A. Issa and K. A. Aadim, “Influence of Laser Energy on Structural and Optical Properties of ZnO(x):NiO(1−x) Films Prepared by Pulse Laser Deposition,” J. Opt., 2024.

[41] C. W. Kung, H. W. Chen, C. Y. Lin, R. Vittal, and K. C. Ho, “Synthesis of Co3O4 nanosheets via electrodeposition followed by ozone treatment and their application to high-performance supercapacitors,” Journal of Power Sources, vol. 214, pp. 91-99, 2012.

[42] Zhang, Y. Liu, and X. Chen, “Room-temperature gas sensors based on Co3O4 nanostructures: A review of recent advances,” Sensors and Actuators B: Chemical, vol. 398, 134726, 2024.

[43] A. A. Kamil, N. A. Bakr, T. H. Mubarak, and J. Al-Zanqanawee, “Effect of Au and Ag nanoparticles addition on the morphological, structural and optical properties of ZnO thin films deposited by sol-gel method,” Journal of Ovonic Research, vol. 18, no. 3, pp. 431-442, 2022.

[44] R. S. Dubey, R. H. Krishna, and S. R. S. Prabaharan, “Co3O4 thin films deposited by pulsed laser deposition: Effect of substrate temperature on structural and electrochemical properties,” Materials Science in Semiconductor Processing, vol. 165, 107678, 2023.

[45] A. A. Kamil, N. A. Bakr, T. H. Mubarak, and J. Al-Zanqanawee, “Synthesis and study of the optical and structural properties of Au and Ag nanoparticles by pulsed laser ablation (PLAL) technique,” Digest Journal of Nanomaterials and Biostructures, vol. 16, no. 4, pp. 1219-1226, 2021.

[46] S. S. Chiad, H. A. Noor, O. M. Abdulmunem, and N. F. Habubi, “Optical and structural properties of Ni-doped Co3O4 nanostructure thin films via CSPM,” Journal of Physics: Conference Series, vol. 1362, no. 1, 012115, 2019.

[47] S. K. Gautam, A. Das, S. Ojha, D. K. Shukla, D. M. Phase, and F. Singh, “Electronic structure modification and Fermi level shifting in niobium-doped anatase titanium dioxide thin films: a comparative study of NEXAFS, work function and stiffening of phonons,” Physical Chemistry Chemical Physics, vol. 18, no. 5, pp. 3618-3627, 2016.

[48] D. Thiyagarajan, S. Li, S. Subramani, A. Thirumurugan, and B. K. Lee, “Titanium metal-organic framework-derived nanocrystalline TiO2-supported nitrogen-doped carbon nanostructures as highly efficient antibiotic adsorbents,” Applied Surface Science, vol. 645, 158842, 2024.

[49] A. S. Mohammed and O. A. Fahad, “Sensitivity enhancement for NO2 gas sensor based on Alq3:TiO2,” in AIP Conference Proceedings, vol. 2372, no. 1, p. 040008, 2021.

[50] R. S. Ali, H. S. Rasheed, N. F. Habubi, and S. S. Chiad, “Synthesis and characterization of manganese-doped FeS2 thin films via chemical spray pyrolysis,” Chalcogenide Letters, vol. 20, no. 1, pp. 63-72, 2023.

[51] S. Park, H. Kim, and C. Lee, “Enhanced acetone gas sensing performance of Co3O4 nanofibers by La2O3 surface modification,” Ceramics International, vol. 47, no. 10, pp. 14256-14263, 2021.

[52] D. M. Stansel, N. M. Laurendeau, and D. W. Senser, “CO and NOx emissions from a controlled-air burner: Experimental measurements and exhaust correlations,” Combustion Science and Technology, vol. 104, no. 4-6, pp. 207-234, 1995.

[53] A. A. Khadayeir, E. S. Hassan, T. H. Mubarak, S. S. Chiad, N. F. Habubi, M. O. Dawood, and I. A. Al-Baidhany, “The effect of substrate temperature on the physical properties of copper oxide films,” Journal of Physics: Conference Series, vol. 1294, no. 2, 022009, 2019.

[54] J. Zhang, X. Liu, G. Neri, and N. Pinna, “Nanostructured materials for room-temperature gas sensors,” Advanced Materials, vol. 28, no. 5, pp. 795-831, 2016.

[55] Y. Seo, J. Kim, and J. H. Lee, “Room-temperature gas sensing of TiO2-based sensors: A review,” Sensors and Actuators B: Chemical, vol. 357, 131416, 2022.

[56] H. J. Kim and J. H. Lee, “Highly sensitive and selective gas sensors using p-type oxide semiconductors: Overview,” Sensors and Actuators B: Chemical, vol. 192, pp. 607-627, 2014.

[57] A. Dey, “Semiconductor metal oxide gas sensors: A review,” Materials Science and Engineering: B, vol. 229, pp. 206-217, 2018.